CANCER RESEARCH COMMUNICATIONS

AACR American Association for Cancer Research

RESEARCH ARTICLE https://doi.org/10.1158/2767-9764.CRC-23-0275 OPEN ACCESS

WNT4 Regulates Cellular Metabolism via Intracellular Activity at the Mitochondria in Breast and Gynecologic Cancers

Joseph L. Sottnik[1], Madeleine T. Shackleford[1], Sydney K. Robinson[1], Fabian R. Villagomez[2], Shaymaa Bahnassy[3], Steffi Oesterreich[4], Junxiao Hu[5], Zeynep Madak-Erdogan[6], Rebecca B. Riggins[3], Bradley R. Corr[7], Linda S. Cook[8], Lindsey S. Treviño[9], Benjamin G. Bitler[2], and Matthew J. Sikora[1]

ABSTRACT

Wnt ligand WNT4 is critical in female reproductive tissue development, with *WNT4* dysregulation linked to related pathologies including breast cancer (invasive lobular carcinoma, ILC) and gynecologic cancers. WNT4 signaling in these contexts is distinct from canonical Wnt signaling yet inadequately understood. We previously identified atypical intracellular activity of WNT4 (independent of Wnt secretion) regulating mitochondrial function, and herein examine intracellular functions of WNT4. We further examine how convergent mechanisms of *WNT4* dysregulation impact cancer metabolism. In ILC, *WNT4* is co-opted by estrogen receptor α (ER) via genomic binding in *WNT4* intron 1, while in gynecologic cancers, a common genetic polymorphism (rs3820282) at this ER binding site alters *WNT4* regulation. Using proximity biotinylation (BioID), we show canonical Wnt ligand WNT3A is trafficked for secretion, but WNT4 is localized to the cytosol and mitochondria. We identified DHRS2, mTOR, and STAT1 as putative WNT4 cytosolic/mitochondrial signaling partners. Whole metabolite profiling, and integrated transcriptomic data, support that WNT4 mediates metabolic reprogramming via fatty acid and amino acid metabolism. Furthermore, ovarian cancer cell lines with rs3820282 variant genotype are WNT4 dependent and have active WNT4 metabolic signaling. In protein array analyses of a cohort of 103 human gynecologic tumors enriched for patient diversity, germline rs3820282 genotype is associated with metabolic remodeling. Variant genotype tumors show increased AMPK activation and downstream signaling, with the highest AMPK signaling activity in variant genotype tumors from non-White patients. Taken together, atypical intracellular WNT4 signaling, in part via genetic dysregulation, regulates the distinct metabolic phenotypes of ILC and gynecologic cancers.

Significance: WNT4 regulates breast and gynecologic cancer metabolism via a previously unappreciated intracellular signaling mechanism at the mitochondria, with WNT4 mediating metabolic remodeling. Understanding *WNT4* dysregulation by estrogen and genetic polymorphism offers new opportunities for defining tumor biology, precision therapeutics, and personalized cancer risk assessment.

Introduction

The Wnt ligand WNT4, considered a "problem child" among Wnts (1, 2), is broadly critical for organogenesis and development. Complete loss-of-function is lethal *in utero* due to multi-organ dysgenesis/agenesis (1). Beyond fetal development, WNT4 has mechanistically distinct roles in female reproductive tissues, in organogenesis of the ovaries and uterus, female sex differentiation,

[1]Department of Pathology, University of Colorado Anschutz Medical Campus, Aurora, Colorado. [2]Division of Reproductive Sciences, Department of Obstetrics and Gynecology, University of Colorado Anschutz Medical Campus, Aurora, Colorado. [3]Department of Oncology, Lombardi Comprehensive Cancer Center, Georgetown University, Washington, District of Columbia. [4]Department of Pharmacology and Chemical Biology, University of Pittsburgh, Pittsburgh, Pennsylvania. [5]Biostatistics and Bioinformatics Shared Resource, University of Colorado Cancer Center, Aurora, Colorado. [6]Department of Food Science and Human Nutrition, Cancer Center at Illinois, Division of Nutritional Sciences, University of Illinois Urbana-Champaign, Champaign, Illinois. [7]Division of Gynecologic Oncology, Department of Obstetrics and Gynecology, University of Colorado Anschutz Medical Campus, Aurora, Colorado. [8]Department of Epidemiology, University of Colorado School of Public Health, Aurora, Colorado. [9]Depratment of Population Sciences, Division of Health Equities, City of Hope, Duarte, California.

J.L. Sottnik and M.T. Shackleford contributed equally as co-first authors of this article.

B.G. Bitler and M.J. Sikora contributed equally as co-senior authors of this article.

Corresponding Authors: Matthew J. Sikora, University of Colorado Anschutz Medical Campus, Mail Stop 8104, RC1S-5110, 12801 E. 17th Ave., Aurora, CO 80045. E-mail: matthew.sikora@cuanschutz.edu; and Benjamin G. Bitler, benjamin.bitler@cuanschutz.edu

doi: 10.1158/2767-9764.CRC-23-0275

This open access article is distributed under the Creative Commons Attribution 4.0 International (CC BY 4.0) license.

© 2024 The Authors; Published by the American Association for Cancer Research

and pregnancy phenotypes in the uterus and mammary gland. Accordingly, WNT4 dysfunction is associated with reproductive, gynecologic, and endocrine pathologies including precancerous uterine lesions, ovarian cancer, and the breast cancer subtype invasive lobular carcinoma (ILC; reviewed in ref. 1). Though WNT4 engages cell- and tissue-specific downstream pathways that are not well defined, converging phenotypes in reproductive tissues and associated cancers suggest that understanding WNT4 regulation and signaling can provide new insights into cancers primarily affecting women.

In the mammary gland, WNT4 is critical for ductal elongation and branching during pregnancy. In this context, *WNT4* expression is induced by progesterone in progesterone receptor (PR)-positive luminal cells, and WNT4 protein subsequently signals in a paracrine manner, mediating stem cell proliferation and renewal likely via β-catenin–dependent signaling (3). We found that in ILC cell lines, *WNT4* expression is co-opted and directly controlled by estrogen receptor α (ER), and that WNT4 is necessary for ER-driven growth and antiestrogen resistance in ILC cell lines (4–6). However, owing to the hallmark loss of E-cadherin (7), ILC cells and tumors typically lack β-catenin protein and fail to engage β-catenin–dependent Wnt signaling (5, 7). We found that ER-driven WNT4 instead controls mTOR signaling and mitochondrial dynamics in ILC cells; WNT4 knockdown compromises respiratory capacity leading to cell death (6). This phenotype is putatively linked to the unique metabolism of ILC, which are considered metabolically quiescent versus invasive ductal carcinoma (IDC, i.e., breast cancer of no special type). Clinical ILC imaging shows reduced glucose uptake, as ILC tumors have approximately 40% reduced glucose uptake versus IDC in ^{18}F-fluorodeoxyglucose (FDG)/PET-CT imaging (8–13), and ILC tumors with no detectable FDG uptake are common especially in metastatic ILC (9, 13, 14). Compared with IDC, expression of glucose metabolism genes are reduced in ILC (15), and tissue microarray studies show ILC express lower levels of related proteins (e.g., GLUT1/*SLC2A1*; ref. 16). Conversely, ILC tumors show differential expression of lipid metabolism–related proteins (15, 17), and accordingly, studies with antiestrogen-resistant ILC models identify increased lipid and glutamate metabolism as critical to the resistant phenotype (18–20). Taken together, these observations suggest that ER$^+$ ILC cells and tumors have a distinct metabolic phenotype compared with other breast cancers, which our work links directly to WNT4-dependent signaling activity. With cancer metabolism increasingly tractable as a treatment target, there is an urgent need to better define WNT4-mediated mechanisms of metabolic reprogramming.

Paralleling the essential role of WNT4 in mammary gland development, WNT4 dysregulation is associated with female-to-male sex reversal phenotypes, uterine agenesis, and ovarian dysgenesis (1). Strikingly, over 20 genome-wide association studies link SNPs at the *WNT4* locus to increased risk of gynecologic pathologies including endometriosis and ovarian cancer (1). Fine mapping and functional studies identify SNP rs3820282, a C>T transition in *WNT4* intron 1, as the likely pathogenic SNP (21, 22). Of note, the rs3820282 variant allele frequency (VAF) varies from 0% to over 50% across racial/ethnic populations (23). The rs3820282 variant creates a binding site for nuclear receptor-class transcription factors, also converting a half estrogen-response-element (ERE) to a full consensus ERE (5, 22). Importantly, knock-in of the variant allele in mice is sufficient to increase *Wnt4* expression in gynecologic tissue *in vivo* (*bioRxiv* 2022.10.25.513653). We also showed that this locus is directly bound by ER in ILC cells [wild-type (WT) for rs3820282] but not other breast cancer cells (5). These observations suggest convergent mechanisms of dysregulated *WNT4* gene expression, via ER and genetic polymorphism, respectively drive breast and gynecologic pathologies.

Toward understanding WNT4 signaling, we previously showed in ILC and ovarian cancer cells that WNT4 signals independent of canonical Wnt secretion and paracrine activity via an atypical intracellular mechanism (6, 24). In this study, we used proximity biotinylation to profile WNT4's interactome, signaling partners, and intracellular localization. We also used global untargeted mass spectrometry (MS)-based metabolomics analyses to profile the metabolic effects of WNT4 regulation and signaling. We performed reverse phase protein array (RPPA) analyses of 103 primary human gynecologic tumors, enriched for patient diversity and germline rs3820282 variant genotype, to determine the impact of the rs3820282/*WNT4* axis on tumor biology. These analyses corroborate a previously unappreciated role for WNT4 in regulating cellular respiration, in lipid and amino acid metabolism, and in metabolic remodeling of ILC and gynecologic cancers.

Materials and Methods

Cell Culture

MDA MB 134VI (MM134; RRID:CVCL_0617), SUM44PE (44PE; RRID:CVCL_3424), HT1080 (RRID:CVCL_0317), and HT1080-A11 (*PORCN*-knockout, -PKO) were maintained as described previously (4, 24). WNT4 overexpressing models (W4OE) and WNT3A overexpressing models were described previously and cultured in the same conditions as parental cell lines (24). Ovarian cancer cell lines, OVCA429 (RRID:CVCL_3936), OVCAR2 (RRID:CVCL_3941), OVCAR3 (RRID:CVCL_0465), 41M (RRID:CVCL_4993, known derivative of OAW28), OVCA432 (RRID:CVCL_3769), OVSAHO (RRID:CVCL_3114), DOV13 (RRID:CVCL_6774), CAOV3 (RRID:CVCL_0201), were maintained as described previously (25, 26). Wnt-BirA fusion expressing lines (described below) were also cultured as the parental cells. All lines were incubated at 37°C in 5% CO_2.

MM134 were originally sourced from ATCC (HTB-23) in 2016. 44PE were originally sourced from Asterand/BioIVT (HUMANSUM-0003004) in 2016. HT1080 and -PKO derivative were a generous gift from Dr. David Virshup in 2017. Ovarian cancer cell lines were obtained from the U. Colorado Gynecologic Tissue and Fluid Bank (GTFB) in 2021. Cell lines are authenticated annually via autosomal short tandem repeat profiling with the University of Arizona Genetics Core cell line authentication service, and confirmed *Mycoplasma* negative (Lonza MycoAlert) every 4 months (most recently confirmed negative in September 2023). Authenticated cells were in continuous culture <6 months.

17β-Estradiol (E2; catalog no. 2824), Z-4-hydroxytamoxifen (4OHT; catalog no. 3412), and fulvestrant (fulv/ICI182,780; catalog no. 1047) were obtained from Tocris Bioscience (Bio-Techne) and dissolved in ethanol. Everolimus (evero; catalog no. 11597) and PF-4708671 (PF; catalog no. 15018) were obtained from Cayman Chemical and dissolved in DMSO.

siRNAs were reverse transfected using RNAiMAX (Thermo Fisher Scientific) according to the manufacturer's instructions. All constructs are siGENOME SMARTpool siRNAs (Dharmacon/Horizon Discovery), nontargeting pool #2 (D-001206-14-05), human *WNT4* (M-008659-03-0005), human *ESR1* (M-003401-04-0010); each pool includes four individual siRNA constructs. Knockdown validation, validation of pooled constructs, and siRNA efficacy in ILC cells for siWNT4 and siESR1 are described previously (5, 6, 27).

Cell proliferation was assessed via double-stranded DNA (dsDNA) quantification by hypotonic lysis and Hoescht 33258 fluorescence as described previously (24).

Proximity-dependent Biotinylation

WNT3A and WNT4 were subcloned by Gateway recombination from the open-source Wnt library (Addgene Kit #1000000022) to the MAC-Tag-C vector (Addgene #108077; ref. 28), generating Wnt open reading frame (ORF) with C-terminal BirA fusion (Wnt-BirA). The Wnt-BirA ORF was subcloned into pLenti-CMV-Blast-empty (Addgene #17486) by BamHI-XhoI double digest, generating pLenti-CMV_Wnt-BirA plasmids, which were validated by complete plasmid sequencing (Mass General Hospital CCIB DNA Core). pLenti-CMV_Wnt-BirA plasmids were packaged for lentiviral transduction, and stably transduced into MM134, HT1080, and HT1080-PKO as described previously (24). For proximity biotinylation analyses, parental and Wnt-BirA cells were treated with 50 μmol/L biotin (MilliporeSigma B4501) for 24 hours. Cells were then lysed with lysis buffer with 1% Triton X-100 [RPPA buffer (6)], and biotinylated proteins were extracted from the lysates using Pierce Streptavidin Magnetic Beads (Thermo Fisher Scientific 88816) per the manufacturer's instructions.

BioID-MS Analyses

For MS analyses, cell lines (MM134, HT1080, HT1080-PKO; parental, WNT3A-BirA, and WNT4-BirA for each) were plated to 10 cm plates in biological duplicate, and treated with 50 μmol/L biotin for 24 hours. Cells were lysed and extracted as above; sample/bead slurry was submitted for MS analyses at the Central Analytical Mass Spectrometry Facility at the University of Colorado Boulder (Boulder, CO). Detailed description of protein extraction and MS are provided in Supplementary Methods S1.

Label-free quantification (LFQ) data from MaxQuant were processed using LFQ-Analyst (29) to define differentially enriched proteins across Wnt-BioID (proximity-dependent biotinylation) studies. For comparisons, missing/zero values were imputed using Perseus-type or MinProb algorithms, with downstream hits required to be identified using both methods. Wnt-associated proteins were defined by increased LFQ versus control (parental cells without Wnt-BirA) with adjusted $P < 0.4$. Proteins identified in >20% of studies in the CRAPome database (30) were excluded from further analyses. Gene ontology analyses were performed using Enrichr (31), DAVID (32), and SubCell BarCode ((33), NetWork multi-protein localization tool).

Immunoblotting

Immunoblotting was performed as described previously (6, 24). Blots were probed with Streptavidin-HRP (Cell Signaling Technology #3999; RRID:AB_10830897) or antibodies used according to manufacturer's recommendations: WNT4 (R&D Systems, MAB4751; RRID:AB_2215448); WNT3A (Novus Biologicals, MAB13242); anti-HA-HRP conjugate (Cell Signaling Technology #2999; RRID:AB_1264166); DHRS2 (Sigma HPA053915; RRID:AB_2682307); mTOR (Cell Signaling Technology #2983; RRID:AB_2105622); STAT1 (Sigma HPA000931; RRID:AB_1080100).; MCL1 (Cell Signaling Technology #5453; RRID:AB_10694494); ACC1 (*ACACA*, Abcam ab45174; RRID:AB_867475); ACC1-pS79 (Cell Signaling Technology #3661; RRID:AB_330337); AMPKα (Cell Signaling Technology #2532; RRID:AB_330331); AMPKα-pT172 (Cell Signaling Technology #2535; RRID:AB_331250). We note that recent lots of WNT4 MAB4751 show substantially increased non-specific background relative to our prior studies (6, 24), and can detect overexpressed WNT4 but no longer reliably detect endogenous WNT4 protein.

Metabolomics Analyses

MM134 and OVSAHO cells were transfected with siRNA for 72 hours prior to harvest; MM134 and MM134-W4OE were treated with vehicle (0.6% DMSO), fulvestrant (100 nmol/L), 4OHT (100 nmol/L), everolimus (100 nmol/L), or PF-4708671 (30 μmol/L) for 48 hours prior to harvest. At harvest, cells were trypsinized and counted, then washed three times in PBS, and frozen as dry cell pellets prior to processing at the University of Colorado Anschutz Medical Campus Cancer Center Mass Spectrometry Shared Resource Core Facility (RRID:SCR_021988). Metabolite extraction and MS details are provided in Supplementary Methods S1. Metabolite data were analyzed using Metaboanalyst 5.0 (34); parameters for specific analyses described in text and in "readme" sheets in associated Supplementary Data (see below).

Metabolic Assays

XF96 (Agilent Technologies, 102417-100) extracellular flux assay kits were used to measure oxygen consumption rate (OCR) and glycolytic flux [extracellular acidification rate (ECAR)] as described previously (35). MM134 cells were reverse transfected with siRNA as above, and 24 hours later, cells were collected by trypsinization and replated to an XF96 microplate at 80k cells/well in 6 biological replicate wells per condition. Twenty-four hours after replating (i.e., 48 hours after siRNA transfection), medium was replaced with Seahorse XF media (Agilent Technologies, 102353-100) and the plate was incubated at 37°C for 30 minutes. After incubation, metabolic flux analyses were performed both at basal conditions and after injection of 5 mg/mL oligomycin (Sigma-Aldrich, 871744), 2 mmol/L FCCP (Sigma-Aldrich, C2920), 5 mmol/L Antimycin A (Sigma-Aldrich, A8774), and 5 mmol/L rotenone (Sigma-Aldrich, R8875; chemicals generously provided by the Jordan Laboratory, CU Anschutz). Outputs were normalized to total cell number.

Extracellular lactate was measured by Lactate-Glo assay (Promega, J5021). MM134 were reverse transfected with siRNA as above in 96-well plates (25k cells/well), and incubated for 6 hours at 37°C prior to time 0. At the indicated timepoints, 3 μL of medium collected and diluted in PBS (1:250 dilution). At time course completion, samples were mixed 1:1 in assay sample buffer, and read per the manufacturer's instructions.

Gynecologic Tumor Cohort and RPPA

The University of Colorado has an Institutional Review Board–approved protocol in place to collect tissue from gynecologic patients with both malignant and benign disease processes. All participants are counseled regarding the potential uses of their tissue and sign a consent form approved by the Colorado Multiple Institutional Review Board (COMIRB, Protocol #07-935). Patients are consented prior to surgery at a clinical visit. Primary gynecologic tissues are collected from patients undergoing surgical resection for a suspected gynecologic malignancy. Blood and tissues are evaluated in the Department of Pathology and then processed at the GTFB laboratory within 2 hours of surgical resection. DNA is isolated from the blood using the DNeasy columns (Qiagen). DNA and tissues are snap frozen and stored at −80°C. Specimens were selected from banked GTFB tissues based on patient ethnicity and tumor types. Patient sample studies herein were approved as non-human subjects research under COMIRB protocol #07-935 and conducted per University of Colorado ethics policies.

Snap frozen tumors were sent to MD Anderson Functional Proteomics RPPA Core Facility (RPPA Core Facility RRID:SCR_016649). Tumor protein lysates were arrayed on nitrocellulose-coated slides. Sample spots were probed with 484 unique antibodies and visualized by DAB colorimetric reaction to produce stained slides. Relative protein target levels were determined for each and designated as $\log_2$ intensities and subsequently median-centered. Level 4 data (i.e., normalized for loading and batch effects) was used for analyses. Differential target levels were assessed using Morpheus (https://software.broadinstitute.org/morpheus) signal to noise analysis, further described in associated data files.

SNP Genotyping

Cell line gDNA and tumor gDNA from the GTFB were genotyped for rs3820282 using TaqMan assay C__27521414_20 (Thermo Fisher Scientific #4351379) and TaqMan genotyping master mix (Thermo Fisher Scientific #4371353). Reactions were carried out on a Thermo Fisher Scientific QuantStudio6 Real-Time PCR System, and genotype calls were made using QuantStudio analysis software.

Statistical Considerations

Analyses were completed using Prism GraphPad (v10) and proper implementation of statistical analyses was overseen by Dr. Junxiao Hu. Specific statistical tests are reported in the text and figure legends.

Data Availability

All of the protein array and metabolomics data are available in the Supplementary Data.

Results

WNT4-BioID Identifies Distinct WNT4 Intracellular Localization to the Mitochondria

Our prior work supports that intracellular WNT4 activity regulates mitochondrial function (6, 24), but WNT4 localization and signaling partners for intracellular signaling are unknown. To profile WNT4 trafficking, localization, and novel intracellular functions, we performed BioID followed by MS. We expressed WNT4 or WNT3A fused to C-terminal BirA biotin ligase in HT1080 WT and porcupine O-acetyltransferase (*PORCN*)-knockout (PKO) cells (Wnt-responsive fibrosarcoma cell line), and ILC cell line MDA MB 134VI (MM134; Supplementary Fig. S1A–S1C). Use of PKO cells allowed us to validate that BioID with Wnt overexpression appropriately maps Wnt trafficking (discussed below), and we previously identified WNT4 intracellular signaling and trafficking in each of these models (6, 24). Cells were biotin-treated for 24 hours, and biotinylated proteins—that is, those within approximately 10 nm of Wnt-BirA (Supplementary Fig. S1C)—were extracted and profiled by MS. Raw data for BioID-MS are provided in Supplementary Data S1.

We confirmed our BioID-MS approach could identify differential canonical WNT3A trafficking based on PORCN status (HT1080 vs. HT1080-PKO; Supplementary Fig. S1D). In canonical Wnt trafficking, PORCN is required for Wnt interaction with Wntless (WLS) in the endoplasmic reticulum, subsequent WLS-mediated Wnt trafficking through the Golgi, and Wnt secretion; PORCN ablation inhibits Wnt trafficking and secretion. Comparing WNT3A-associated proteins in HT1080 versus HT1080-PKO (Supplementary Data S2), $n = 46$ putative PORCN-dependent WNT3A-associated proteins included WLS (enriched >20-fold in HT1080 vs. HT1080-PKO; Supplementary Fig. S1E), and were enriched for Golgi localization (GO Cellular Compartment: trans-Golgi network, $P = 0.0024$). These enrichments confirm that BioID identified suppression of WNT3A trafficking to the Golgi in PKO cells. Only $n = 8$ WNT4-associated proteins were enriched in HT1080 versus HT1080-PKO, suggesting PORCN-knockout had little impact on WNT4 trafficking, consistent with our prior report of atypical (PORCN-independent) WNT4 trafficking (24).

We compared WNT4-associated ($n = 277$) versus WNT3A-associated ($n = 184$) proteins in HT1080 (Fig. 1A). From the WNT4-specific proteins in HT1080 ($n = 172$), we also identified "high-confidence" WNT4-associated proteins based on increased signal for WNT4-BioID, versus control and WNT3A-BioID, in at least two of three cell lines ($n = 72$; Fig. 1A and B; Supplementary Data S2). From these subsets, we examined differential predicted localization using gene ontology and SubCell BarCode analysis (ref. 33; Supplementary Data S2). Consistent with canonical Wnt secretion, WNT3A-associated proteins were enriched for localization at the ER/Golgi (Fig. 1C), and WNT3A-predicted localization was in the secretory pathway (Fig. 1D). In contrast, WNT4-associated proteins were enriched for mitochondrial proteins (Fig. 1C; Supplementary Data S2). Using SubCell barcode analysis, WNT4 predicted localization was in the cytosol or at the mitochondria (Fig. 1D). High-confidence WNT4-associated proteins were also enriched for mitochondrial proteins and predicted WNT4 localization at the mitochondria (Fig. 1B–D). High-confidence WNT4-associated proteins included mitochondrial membrane and matrix proteins (Fig. 1E, red text) as well as proteins involved in mitochondrial biogenesis/dynamics (Fig. 1E, pink text), supporting mitochondrial WNT4 localization.

Among the most strongly enriched putative WNT4-associated proteins were mitochondrial reductase/dehydrogenase DHRS2, regulators of mitochondrial biogenesis, dynamics, and mitophagy (PIK3C3, PIK3R4, and mTOR), and STAT1, which can translocate to the mitochondria to regulate cellular metabolism (36–38). For DHRS2, mTOR, and STAT1, we validated the putative association with WNT4 by streptavidin pulldown and immunoblotting in independent samples, that is, pulldown of biotinylated DHRS2/mTOR/STAT1 was enriched in WNT4-BioID cells versus WNT3A-BioID or control cells (Fig. 1F). These data support our BioID-MS findings and a novel role for WNT4 in regulating cellular metabolism and mitochondrial function.

Integrated Transcriptome and Metabolome Data Support WNT4 as a Mediator of ER Metabolic Signaling

As the mitochondria are essential for many metabolic processes, we next examined how WNT4 controls metabolism in the context of dysregulated *WNT4* expression, using untargeted MS-based metabolomics in ILC cell line MM134. MM134 are WT for the rs3820282 SNP (discussed below), but *WNT4* expression is aberrantly induced by ER in ILC cell lines—in the normal mammary gland and IDC cell lines, *WNT4* is directly PR controlled, independent of ER (3, 5). Figure 2A summarizes the overall metabolomics study design. We targeted ER-WNT4 signaling directly using siRNA, and in parallel, compared inhibition of ER-WNT4 signaling in parental MM134 versus W4OE MM134 cells.

To first examine the role for ER in regulation of metabolism in ILC cells, we integrated metabolomics data with transcriptomic data in MM134 [GSE171364 (27)], and performed joint pathway analysis of metabolites ($n = 63$) and genes dysregulated by *ESR1* siRNA ($n = 5{,}322$; Fig. 2B; Supplementary Data S3). Consistent with the central role for ER in cell proliferation, integrated pathway analysis showed enrichment in biosynthetic pathways, as well as glycolysis, the

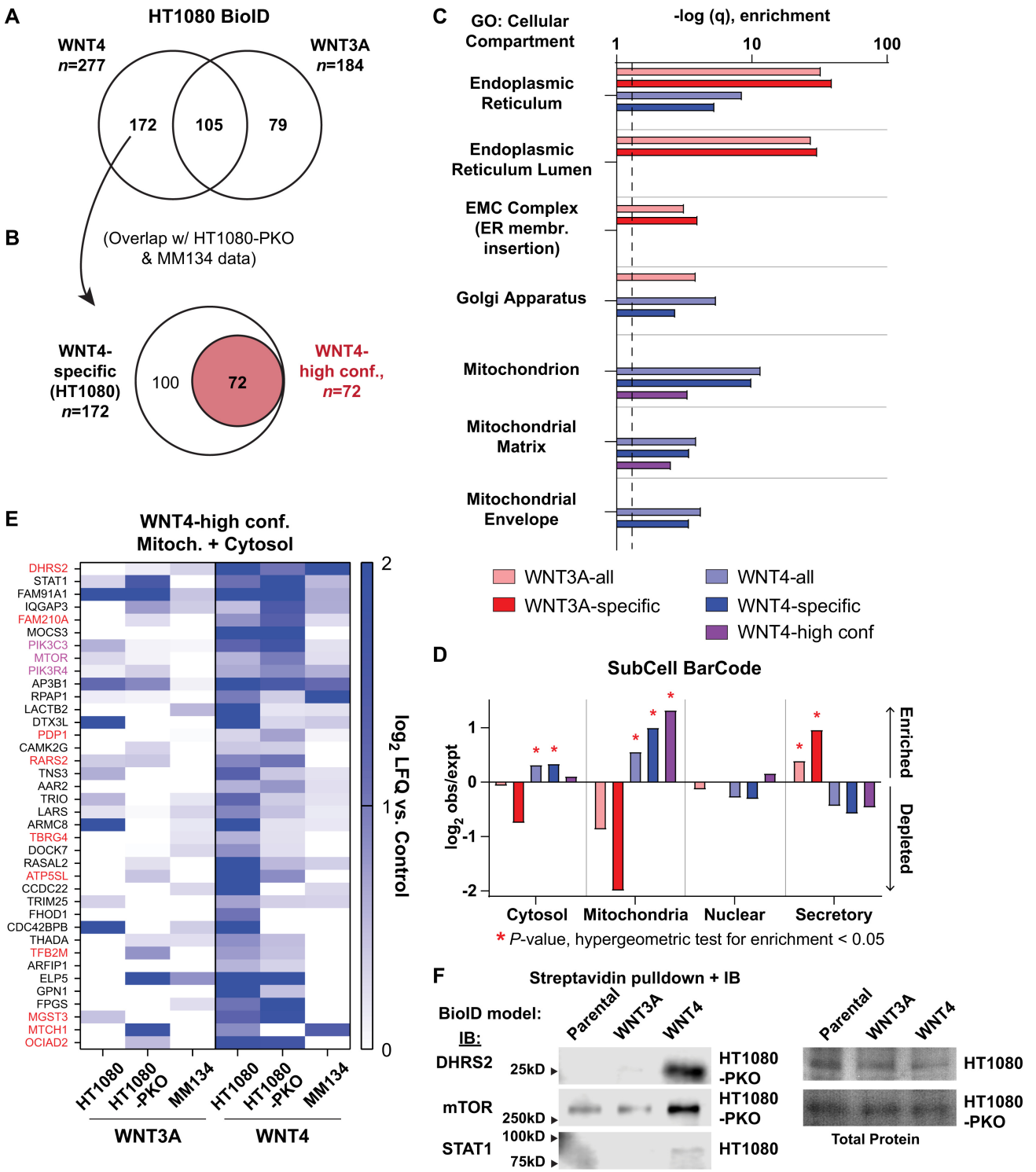

FIGURE 1 BioID supports WNT4 localization to the mitochondria. **A,** Proteins enriched in HT1080 Wnt-BirA versus parental HT1080 cells lacking BirA construct expression. **B,** Overlap of proteins identified in HT1080 (A) versus HT1080-PKO and MM134 identifies $n = 72$ "high-confidence" WNT4-associated proteins. **C,** Gene ontology analysis for cellular compartment for WNT3A- versus WNT4-associated proteins. Dashed line = 1.3 ($P = 0.05$). **D,** Network analysis of WNT3A- versus WNT4-associated proteins via subcell barcode. Enrichments against cell line HCC287 background shown; parallel results observed with other cell line background data, for example, MCF7. **E,** Proteins with predicted cytosolic or mitochondrial localization (subcell barcode) among "high-confidence" WNT4-associated proteins. Red = predicted mitochondrial localization, pink = mTOR complex in mitochondrial dynamics, biogenesis, and autophagy. **F,** Biotin treatment and streptavidin pulldown was performed as for MS studies, and candidate WNT4-associated proteins from E detected by immunoblotting. Total protein by Ponceau.

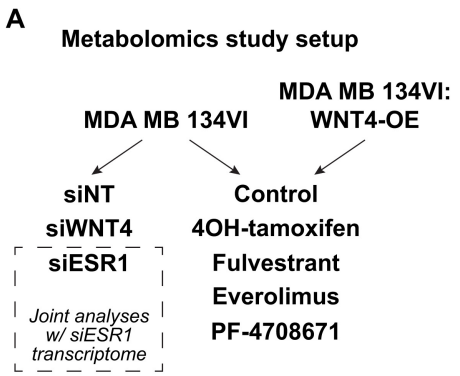

B

siESR1: Metabolome + Transcriptome Metabolic Pathway Enrichment

	Metabolites	Genes	q
Purine metabolism	9	41	1.61E-09
Glycerophospholipid metabolism	4	19	1.63E-08
Glycerolipid metabolism	2	12	0.00404
Val/Leu/Ile degradation	2	19	2.6E-05
Pyrimidine metabolism	4	21	3.1E-05
Glycolysis / Gluconeogenesis	3	19	7.4E-05
Fatty acid metabolism	10	22	4.34E-09
Biosyn. of unsaturated fatty acids		11	0.00044
Fatty acid degradation		13	0.00444
Fatty acid biosynthesis		6	0.00549
Citrate cycle (TCA cycle)	5	10	0.00177

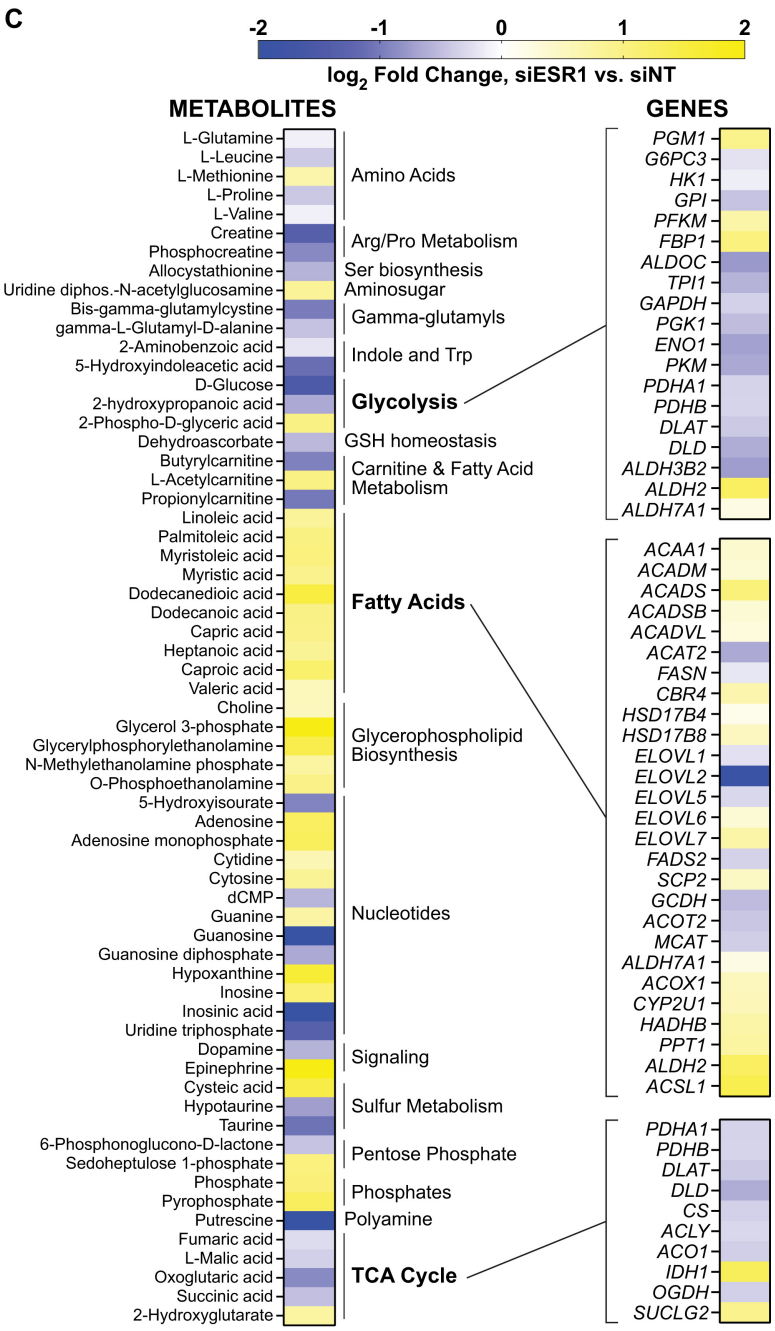

FIGURE 2 ER regulates glycolysis, oxidative phosphorylation, and fatty acid metabolism in ILC cells. **A,** Overall metabolomics study design in MDA MB 134VI ILC cells; all samples in biological triplicate. **B,** Joint analysis of transcriptome + metabolome data identifies dysregulated pathways after ER knockdown. Transcriptome data from GSE171364. **C,** Metabolites levels altered by ER knockdown (left, $n = 63$), with gene expression changes associated with major metabolic mechanisms (right).

tricarboxylic acid (TCA) cycle, and fatty acid metabolism (Fig. 2B). Metabolite and gene expression changes after ER knockdown were consistent with decreased glycolysis and cellular respiration, and increased fatty acid metabolism (Fig. 2C). Notably, while levels of most TCA cycle metabolites and associated genes decreased upon ER knockdown, expression of *IDH1* and level of onco-metabolite 2-hydroxyglutarate increased after ER knockdown (no *IDH1/2* mutations have been reported in MM134 cells). Overall, these data are consistent with reports on the critical role for ER in regulating cellular metabolism in ER^+ breast cancer cells and confirm metabolic remodeling upon suppression of ER.

We next compared effects of ER versus WNT4 knockdown. *WNT4* siRNA broadly dysregulated metabolite levels ($n = 77$; Fig. 3A; Supplementary Data S3), consistent with our report of metabolic dysfunction upon WNT4 knockdown (6). Metabolites dysregulated by WNT4 knockdown extensively mirrored ER knockdown (Fig. 3A and B). Among $n = 46$ metabolites dysregulated

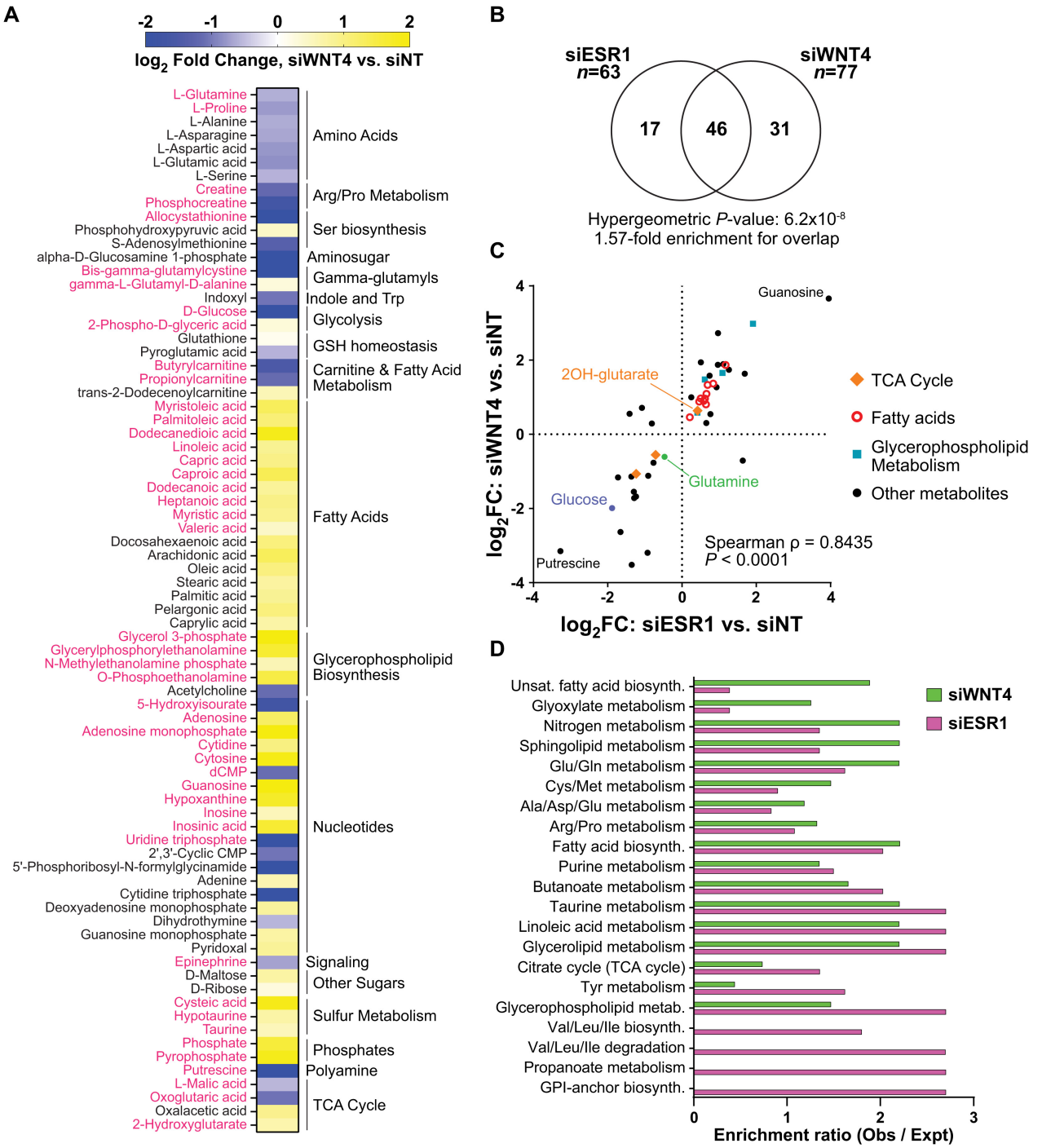

FIGURE 3 Metabolic effects of WNT4 knockdown mirror ER knockdown but have expanded impact on fatty acid and amino acid metabolic pathways. **A,** Metabolite levels altered by WNT4 knockdown ($n = 77$); pink text indicates a shared affected metabolite with ER knockdown. **B,** Metabolites dysregulated by WNT4 versus ER knockdown are strongly enriched for overlap. **C,** WNT4 versus ER knockdown effects on metabolite levels are strongly directly correlated, suggesting an overall parallel effect on ILC cell metabolism. **D,** Pathway analysis with ER metabolites (C) and WNT4 metabolites (Fig. 4A); $P < 0.4$ in ER and/or WNT4 dataset shown.

by both WNT4 and ER knockdown (e.g., fatty acids, 2-hydroxyglutarate, glutamine), siWNT4/siESR1 effects were strongly correlated (Spearman $\rho = 0.8435$; Fig. 3C), supporting that WNT4 is a downstream mediator of ER-driven metabolic regulation. Pathway analysis confirmed that WNT4 and ER knockdown similarly impacted biosynthetic and metabolic pathways (Fig. 3D), for example, TCA cycle, fatty acid biosynthesis, and glutamate metabolism. WNT4 knockdown impacted the levels of more metabolites in pathways including unsaturated fatty acid biosynthesis (pathway enrichment: siESR1,

$P = 0.79$; siWNT4, $P = 0.033$) and glutamine/glutamate metabolism (siESR1, $P = 0.26$; siWNT4, $P = 0.017$; Supplementary Data S3). While the metabolic impact of ER and WNT4 knockdown are tightly correlated, these differences suggest that some metabolic activities of WNT4 signaling are distinct from global transcriptomic and metabolic impacts of ER.

WNT4 Knockdown Dysregulates Cellular Respiration but not Glycolysis

We further examined the differential impact of ER versus WNT4 knockdown on cellular energetics using Seahorse metabolic flux analysis in MM134 cells (Fig. 4A). Paralleling the observed effects on gene expression and metabolite levels in the TCA cycle, *ESR1* or *WNT4* siRNA suppressed basal OCR (Fig. 4A and B). With ER knockdown, cells retained full spare respiratory capacity, likely consistent with a reduction in metabolic activity without compromising capacity. Conversely, WNT4 knockdown caused a decrease in spare respiratory capacity (Fig. 4B); this observation supports that WNT4 knockdown causes mitochondrial dysfunction (6). Unlike the effects of WNT4 knockdown on respiration, we noted siWNT4 had only a modest impact on ECAR versus siESR1 (Fig. 4C). Accordingly, in metabolomics data, siESR1 reduced intracellular lactic acid levels while siWNT4 had no effect compared with control (Fig. 4D), which we also observed measuring lactic acid secretion (Fig. 4E). The differential effect on ECAR and lactic acid levels support that WNT4-mediated metabolic regulation is likely independent of glycolytic activity.

Because WNT4 knockdown suppresses ILC cell ATP levels and dysregulates oxygen consumption/respiration, but not glycolysis, we hypothesized that ILC cells are relatively more reliant on oxidative phosphorylation (OXPHOS) versus glycolysis for energy production. In cellular dependency screens [Depmap (39)], ILC cell lines are uniquely sensitive to suppression of genes involved in pyruvate metabolism. We examined 15 genes in glucose metabolism and pyruvate synthesis in 25 ER^+ cell lines. ILC cell lines ($n = 3$; MM134, 44PE, MM330) were among the most sensitive to knockdown of genes in this pathway (Fig. 4F) and clustered independently from other ER^+ lines (Fig. 4G, left). ILC-like cell line CAMA1 (27, 40) was similarly sensitive to knockdown of pyruvate production genes (Fig. 4F). This phenotype was specific for pyruvate production as TCA cycle genes (e.g., *OGDH*) were broadly essential across ER^+ breast cancer cell lines (Fig. 4G, right). Taken together, WNT4 signaling is necessary for ILC cellular respiration; glycolysis is maintained with WNT4 knockdown but is insufficient to maintain ILC cell viability, as ILC cells are more dependent on cellular respiration via pyruvate production.

WNT4 Signaling is Integrated in an ER-mTOR Pathway and is Critical for Lipid Metabolism

Our metabolomics study also compared small-molecule inhibition of ER-WNT4 signaling on parental MM134 versus W4OE MM134 (Fig. 5A). We hypothesized that WNT4 overexpression would rescue a subset of inhibitor-mediated metabolic effects and identify direct WNT4 signaling effects. Two-factor analysis (W4OE vs. parental, controlled for drug effect) showed that WNT4 overexpression significantly altered the levels of 71 metabolites (Fig. 5B), of which 38 overlapped with siWNT4. The effects of W4OE versus siWNT4 were inverse for 58% of the 38 metabolites ($n = 22$; Fig. 5C), supporting direct WNT4 regulation of metabolites including glucose, glutamate, 2-hydroxyglutarate, and fatty acids ($n = 7$; Supplementary Data S4).

We further examined whether WNT4 overexpression rescued the metabolic effects of individual inhibitors. The effects of mTOR inhibitor everolimus and S6 kinase inhibitor PF-4708671 on parental versus W4OE cells were strongly correlated (Fig. 5D), suggesting that WNT4 overexpression has limited capacity to override inhibition of downstream signaling. Similarly, the effects of antiestrogen fulvestrant were highly correlated in parental versus W4OE, as WNT4 may be insufficient to overcome complete ER inhibition in ER-dependent breast cancer cells. However, a larger subset of effects of 4OH-tamoxifen was reversed in W4OE cells, consistent with tamoxifen partial agonist activity in these cells (4); incomplete ER inhibition by 4OH-tamoxifen (i.e., tamoxifen resistance) can be partially rescued by WNT4 overexpression. From these data, we identified $n = 38$ metabolites for which effects of ≥ 2 inhibitors were reversed by $\geq 30\%$ (Fig. 5E), which were enriched for fatty esters (i.e., carnitines, $n = 4$, $P = 0.032$), supporting a key role for WNT4 in fatty acid/lipid metabolism.

Integrating WNT4-regulated metabolic pathways in siRNA, overexpression, and inhibitor studies identified 41 metabolites differentially regulated by activation versus suppression of WNT4 signaling (Fig. 6A; Supplementary Data S5). Enrichment analysis of these consensus WNT4-regulated metabolites identified the arginine and proline metabolic pathway, supporting a role for WNT4 signaling in glutamate metabolism. Fatty acid biosynthesis and metabolism were key pathways/metabolites regulated via WNT4 signaling (Fig. 6B).

Our data on ER-WNT4 signaling highlight a putative role for lipid metabolism in the distinct metabolic phenotype of ILC. To examine this in tumor data, we performed gene set enrichment analyses from $n = 1{,}360$ genes differentially expressed in ER^+ Luminal A ILC versus IDC (15). Four of the top eight overrepresented pathways (Wikipathways) were metabolic, with an increase in genes associated with lipid metabolism in ILC (Fig. 6C; Supplementary Data S6). Metabolic pathways were also enriched in Hallmark gene signatures, with an increase in genes associated with adipogenesis and fatty acid metabolism, versus a decrease in genes associated with glycolysis and oxidative Phosphorylation, in ILC versus IDC (Fig. 6C); the latter may also reflect the relative metabolic quiescence of ILC compared with IDC (15). Using fast gene set enrichment analyses (fGSEA), differential gene expression in ILC is consistent with decreased glycolysis and increased fatty acid metabolism (Fig. 6D; Supplementary Data S6). These data support that WNT4 signaling contributes to increased lipid metabolism as part of the distinct metabolic phenotype of ILC.

Genetic Polymorphism at the *WNT4* Locus is Associated with a Distinct Metabolic Phenotype

We next examined rs3820282 genotype as a convergent mechanism of activating WNT4 signaling, paralleling ER regulation of WNT4 signaling in ILC, and based on the increased risk of gynecologic cancer associated with rs3820282 variant genotype (1), we expanded our studies into related models. We genotyped a panel of breast, ovarian, and endometrial cancer cell lines ($n = 58$; Supplementary Data S7). Among breast cancer cell lines, only four of 30 lines carried variant alleles (VAF ~13%). In ovarian and endometrial cancer cell lines, 19 of 28 lines carried variant alleles (VAF ~50%), likely reflecting both the increased diversity of patient ethnicity among these models and a distinct role for this SNP in gynecologic cancer. From these data, we selected four WT and four variant genotype ovarian cancer cell lines to examine the impact of WNT4 knockdown, relative to our prior observations in ILC cells. *WNT4* siRNA strongly suppressed proliferation in rs3820282 variant cell lines but had modest or no effect in WT cell lines, despite 70%–85% reduced *WNT4* mRNA levels in all cell lines (Fig. 7A). The differential effect of WNT4 knockdown suggests variant genotype cells are specifically dependent on WNT4 signaling. To examine activity of WNT4 signaling, we measured levels of MCL1 by immunoblot,

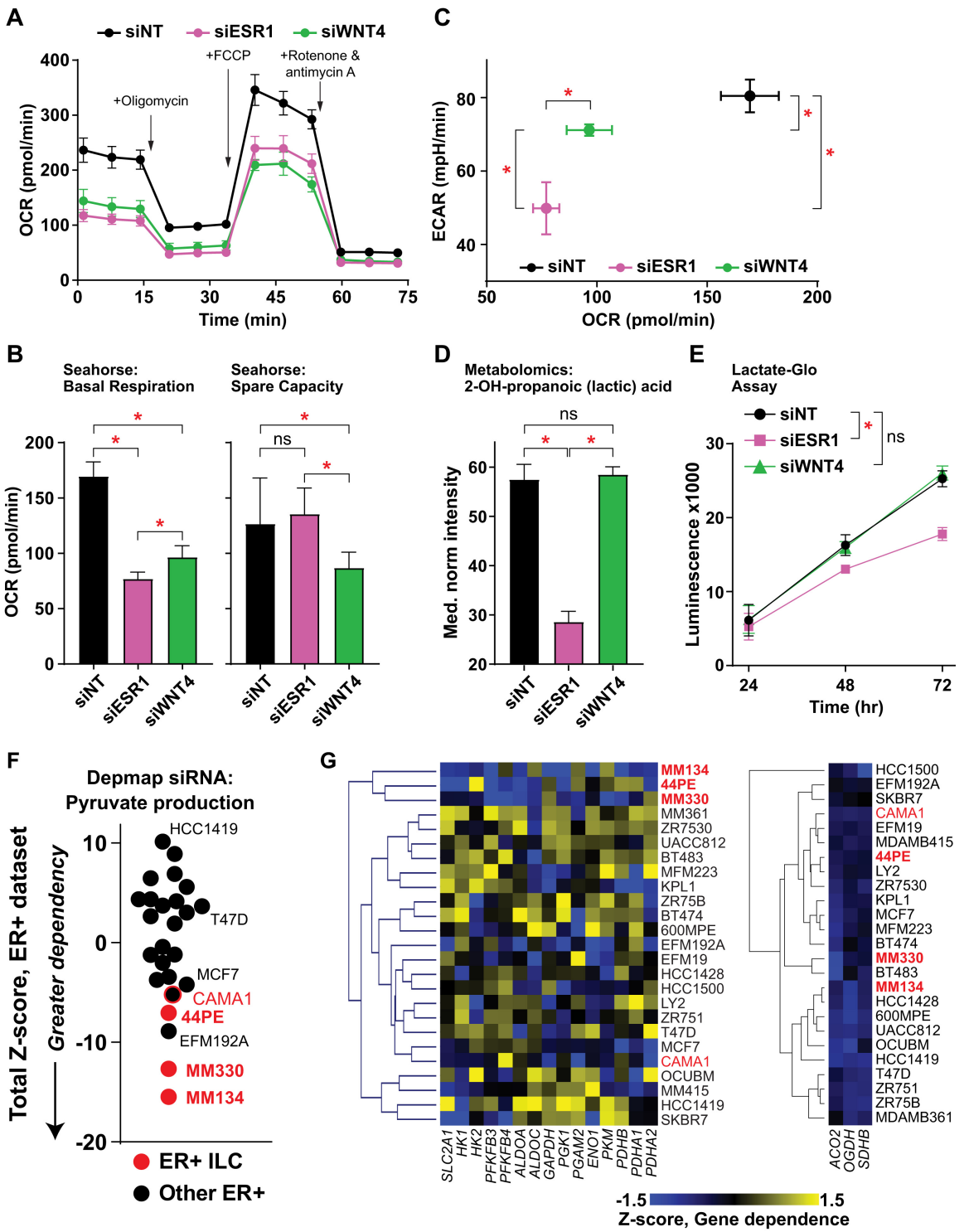

FIGURE 4 WNT4 knockdown impairs respiration but not glycolysis. **A,** Seahorse MitoStress test in MM134. Points represent mean of 6 biological replicates ± SD. **B,** Basal respiration is reduced by ER or WNT4 knockdown, but WNT4 knockdown impairs respiratory capacity. **C,** WNT4 knockdown suppresses OCR, that is, respiration (from B), but has a minimal effect on ECAR, that is, glycolysis. **D,** From metabolomics data, cellular lactic acid levels are reduced by ER knockdown, but not WNT4 knockdown. B–D, comparisons by ANOVA with Dunnett correction. *, adj.$P < 0.05$. **E,** Reduction in lactic acid production was also observed in lactate levels in conditioned medium. *, Two-way ANOVA siRNA effect $P < 0.05$. **F** and **G,** DEMETER2 scores for $n = 15$ genes in pyruvate metabolism [Kyoto Encyclopedia of Genes and Genomes (KEGG) M00001 and M00307] normalized as Z-scores for ER^+ breast cancer cell lines. DEMETER2 siRNA used as ER^+ ILC cell line data are not available in Depmap CRISPR-based screens. CAMA1 denoted separately as an "ILC-like" cell line. F, Total sum of Z-scores for the geneset per cell line. G, Hierarchal clustering for gene Z-scores indicates ER^+ ILC lines as an independent cluster. Pyruvate metabolism genes at left, representative TCA genes at right.

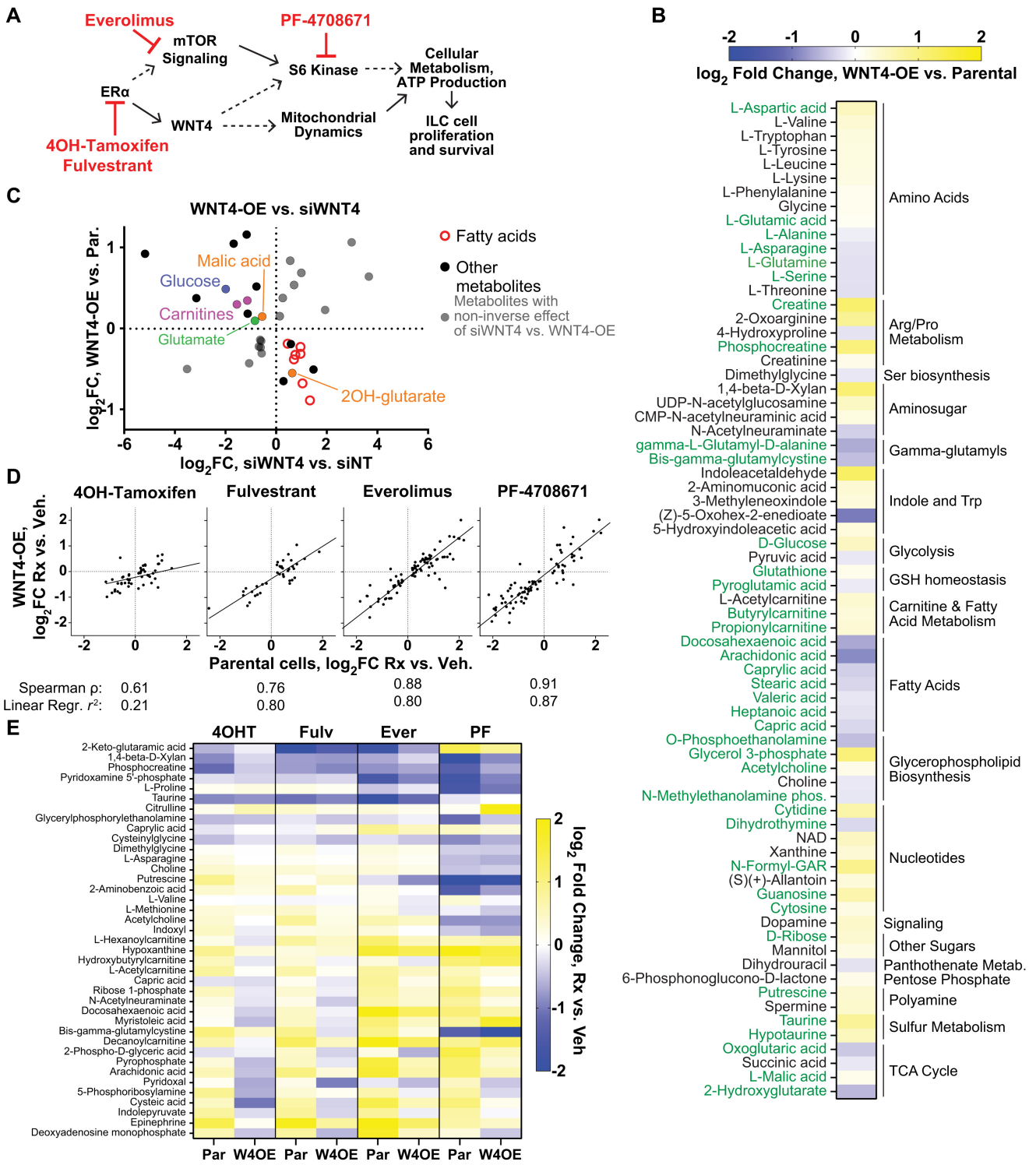

FIGURE 5 WNT4 overexpression rescues some metabolic effects of ER:WNT4 pathway inhibition. **A,** Small-molecule inhibitor targets in current model of ER:WNT4 signaling pathway. **B,** Meta-analysis of parental MM134 cells versus WNT4-OE MM134 across drug treatment series (i.e., WNT4 effect controlled for inhibitor effect) identifies $n = 71$ metabolite levels altered by WNT4 overexpression. Green = overlap with siWNT4 dysregulated metabolites. **C,** Overall changes in metabolite levels caused by WNT4 knockdown versus WNT4 overexpression are inversely correlated, supporting regulation of associated metabolic pathways by WNT4. **D,** Inhibitor effects in parental MM134 versus WNT4-OE MM134 are strongly correlated, but a subset of inhibitor effects are reversed by WNT4 overexpression. **E,** Metabolites for which inhibitor effects is decreased by ≥30% for at least two inhibitors ($n = 39$).

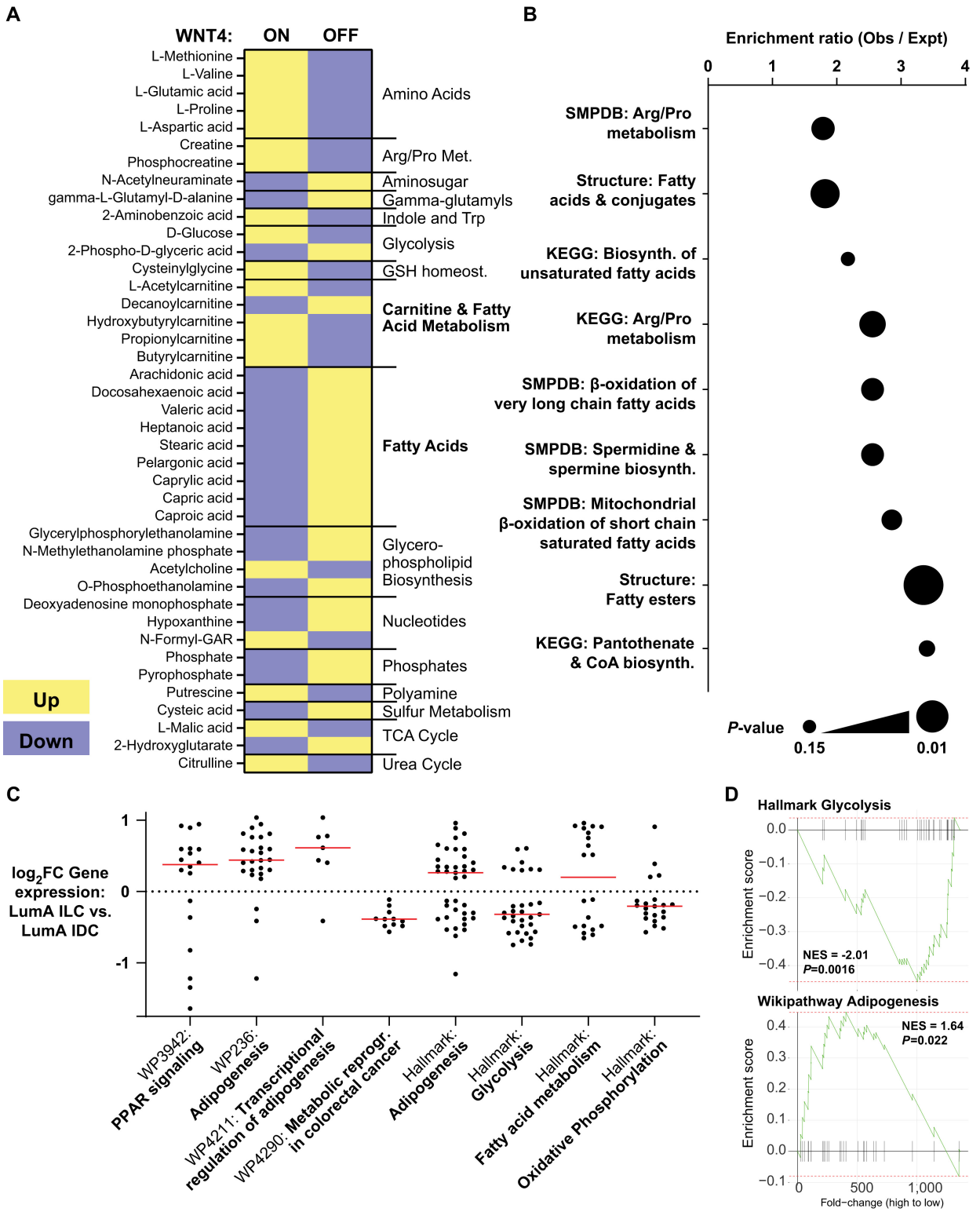

FIGURE 6 Consensus WNT4-regulated metabolites are enriched for fatty acid metabolism. **A,** Consensus of $n = 41$ metabolites rescued with WNT4-OE and metabolites inversely regulated by WNT4-OE versus WNT4 knockdown. WNT4 ON versus OFF corresponds to differential regulation by WNT4 overexpression versus knockdown, respectively. **B,** Pathway analysis of consensus WNT4-regulated metabolites. **C,** Gene set enrichment analysis of genes differentially expressed in Luminal A ILC versus Luminal A IDC ($n = 1360$) includes metabolic pathways, with relative gene expression levels in ILC consistent with increased lipid metabolism and decreased glycolysis and OXPHOS. Points = individual genes (fold changes from TCGA, ref. 7); red bar = median fold change. **D,** fGSEA = fast gene set enrichment analysis of representative pathways in **C**. NES = normalized enrichment score.

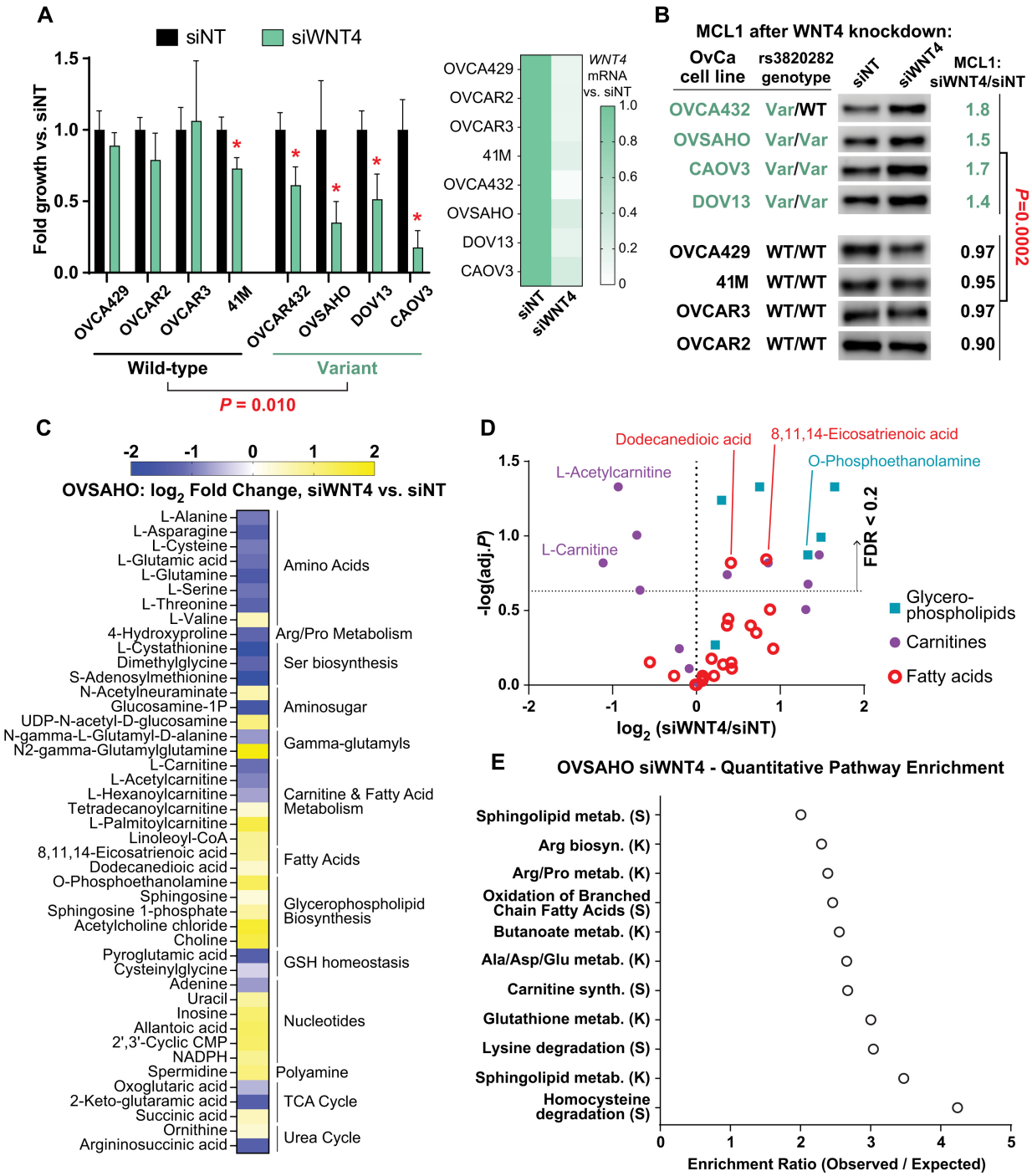

FIGURE 7 WNT4 variant genotype is associated with active WNT4 signaling and metabolic remodeling in ovarian cancer cells. **A,** Left, Proliferation assessed by dsDNA quantification 6 days post-transfection with siRNA (siNT = non-targeting control pool). Bars represent mean of 6 biological replicates ± SD; *, $P < 0.05$, siWNT4 versus siNT, *t* test with Welch correction. WT versus Var model comparison by *t* test of mean fold changes for siWNT4 versus siNT. Right, *WNT4* mRNA by qPCR in parallel samples, 72 hours after siRNA. Mean of biological triplicate, fold change versus siNT. **B,** Lysates harvested 72 hours posttransfection. MCL1 levels assessed by densitometry and normalized to total S6 loading control (6). Fold change in normalized MCL1 levels in Variant versus WT genotype cell lines compared by Student *t* test. **C,** Metabolites dysregulated 72 hours after WNT4 knockdown ($n = 44$), as for MM134. **D,** Fold changes in lipid metabolites. Dashed line on *y*-axis: FDR = 0.2. **E,** Pathway enrichment (Metaboanalyst) for metabolites shown in C; K = KEGG, S = SMPDB.

which we showed increases in ILC cells upon WNT4 knockdown and correlates with mitochondrial dysfunction (6). Consistent with the proliferation results, MCL1 levels specifically increased in variant genotype models after WNT4 knockdown (Fig. 7B). Collectively, these data support that in ovarian cancer cells, WNT4 signaling is specifically active in the context of rs3820282 variant genotype.

To examine WNT4 regulation of metabolism in the context of WNT4-depdendent ovarian cancer cells, we performed untargeted MS-based metabolomics after WNT4 knockdown, as above in ILC model MM134, in ovarian cancer cell line OVSAHO (rs3820282 homozygous variant; Supplementary Data S3). WNT4 knockdown in OVSAHO caused similar dysregulation of consensus WNT4 target metabolites in MM134 cells, including decreased glutamate, decreased carnitines, and increased fatty acids (Fig. 7C). Overall trends in carnitines, fatty acids, and glycerophospholipids in OVSAHO matched those observed in MM134 (Fig. 7D). Pathway enrichment of dysregulated metabolites also mirrored MM134 results, including fatty acid oxidation and glutamate metabolism pathways (Fig. 7E). These data strongly support that the mechanisms by which WNT4 regulates metabolism is shared between ILC and gynecologic cancer, with the latter potentially mediated by the rs3820282 variant genotype.

These observations led us to further explore the role of WNT4 in gynecologic tumor biology, also based on the key roles for WNT4 across reproductive tissues, the convergent mechanisms of *WNT4* dysregulation with rs3820282 versus ER in ILC, and parallels in ILC versus gynecologic cancer biology (1). We leveraged a biobank of snap frozen tissues with matched germline DNA samples via the U. Colorado GTFB. With this resource, we were able to enrich for a diverse patient population to reflect increased VAF in Latinx and East Asian populations (1), and collect sufficient variant genotype tissues for analysis. We performed Taqman SNP genotyping for rs3820282 on genomic DNA samples from $n = 226$ patients, and subsequently selected tissues from 103 patients (Table 1) for RPPA analyses. We enriched the RPPA cohort for germline variant genotypes (heterozygous and homozygous variant, 52%) and samples from non-White patients (47%). Of note, no significant differences in age or BMI were associated with rs3820282 genotype (Table 1).

RPPA data for 484 targets (Supplementary Data S8) were examined for differentially expressed protein networks in tissues from WT versus variant genotype patients as described in Supplementary Data S8. We identified the top 40% of RPPA targets based on differential levels in WT versus variant samples ($n = 194$). Using these targets for hierarchical clustering yielded two major clusters with similar distributions of samples based on tissue type, genotype, and race/ethnicity (Supplementary Fig. S2). STRING network analyses (41) of the RPPA targets differentially increased in rs3820282 WT ($n = 100$) versus variant samples ($n = 94$) identified increased activity of four signaling networks in variant genotype tissues, and five networks in WT genotype tissues (Supplementary Data S8; Supplementary Fig. S3). Several networks converged on metabolic signaling, including activation of an AMPK signaling network in variant genotype tumors (Fig. 8A). Activated AMPK (phospho-AMPKα1 and α2) alone was significantly increased in variant allele tumors (Fig. 8B). Conversely, glucose metabolism networks were increased in WT tumors (Fig. 8C; Supplementary Fig. S3). From these networks, AMPK signaling was inversely correlated with glucose metabolism, with variant genotype tumors showing increased AMPK signaling with decreased glucose metabolism signaling (Fig. 8D). These

TABLE 1 Gynecologic tumor cohort for RPPA analyses total $n = 103$

	Mean (95% CI)
Age at procedure	56.68 (53.92–59.44)
Race	**Subgroup n**
American Indian and Alaska Native	3
Asian	11
Black or African American	16
Multiple race	9
Native Hawaiian/Other Pacific Islander	2
Other	2
Unknown	2
White or Caucasian	58
Ethnicity	**Subgroup n**
Hispanic	12
Non-Hispanic	89
Unknown	2
Race and Ethnicity	**Subgroup n**
White/Caucasian, non-Hispanic	54
Non-White and/or Hispanic, or Unknown	49
Diagnosis	**Subgroup n**
Ovarian high-grade serous	4
Angiolipoma	1
Borderline tumor	3
Carcinosarcoma	5
Cervical carcinoma	1
Cystadenoma	1
Endometrial endometrioid	67
Endometrial mucinous	1
Endometrial serous	3
Leiomyoma	2
Leiomyosarcoma	2
Other	1
Ovarian clear cell	4
Ovarian endometrioid	1
Ovarian mucinous	1
Ovary cyst/Ovary	4
Teratoma	2
	Mean (95% CI)
BMI at time of procedure	32.46 (30.54–34.39)
Wildtype vs. Variant (rs3820282)	**Subgroup n**
Wildtype homozygous	49
Heterozygous	45
Variant homozygous	9
Variant and mean age (95% CI)	**Mean (95% CI)**
Wildtype homozygous	57.1 (52.92–61.29)
Heterozygous	55.84 (51.56–60.13)
Variant homozygous	58.56 (49.57–67.55)
Variant and mean BMI (95% CI)	**Mean (95% CI)**
Wildtype homozygous	31.19 (28.64–33.74)
Heterozygous	33.9 (30.77–37.04)
Variant homozygous	32.2 (23.02–41.37)

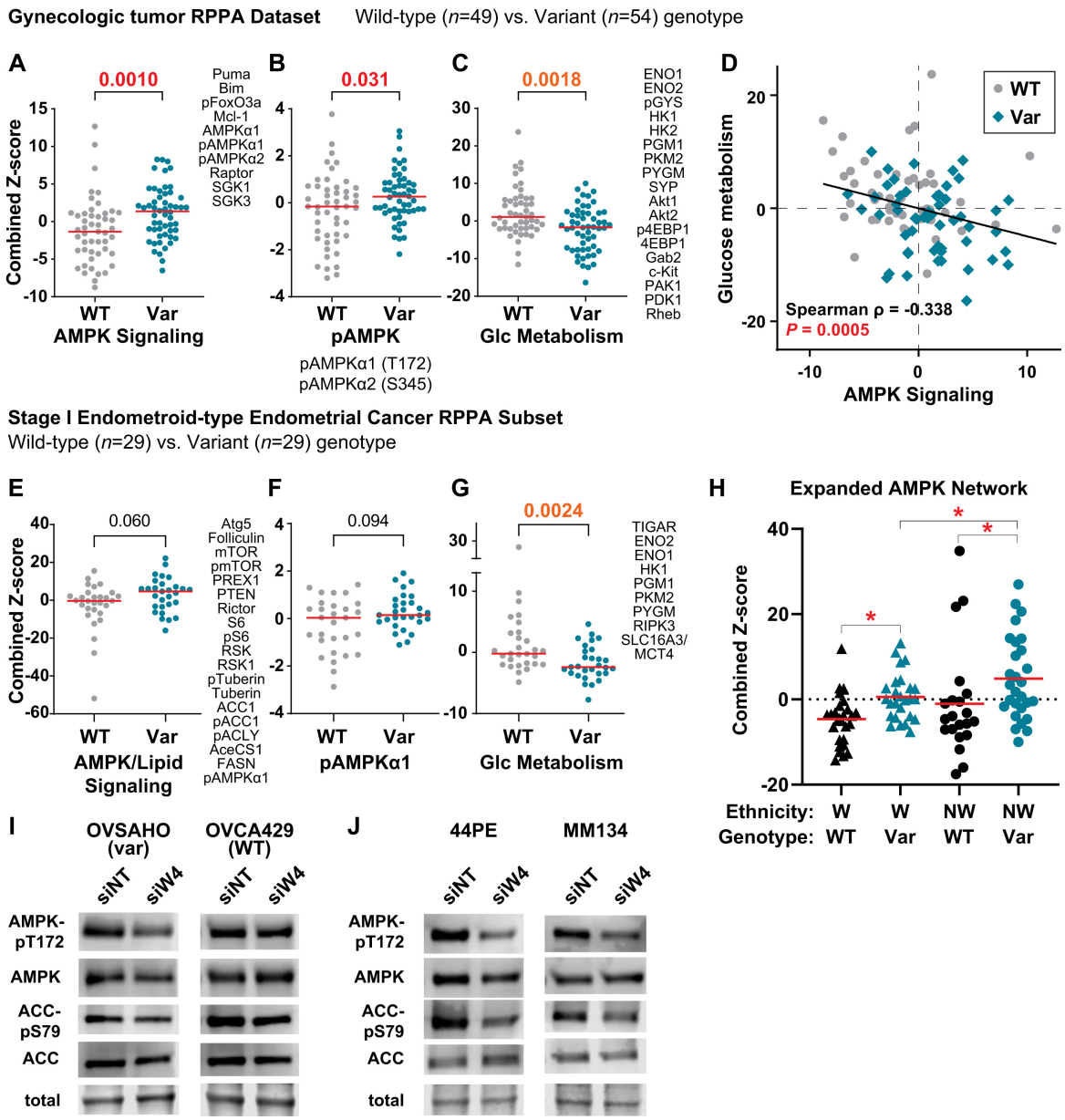

FIGURE 8 WNT4 variant genotype is associated with metabolic remodeling in gynecologic tumors, mirroring ILC signaling. **A–C,** Points represent total network score for the listed RPPA targets for individual tumors based on rs3820282 genotype. Red bar = median score; *P*-value from Mann–Whitney *t* test. **A,** Tumor scores for AMPK-associated network. **B,** Tumor scores for phospho-AMPK only. **C,** Tumor scores for glucose metabolism-associated network. **D,** Scatterplot of network scores in A and C; correlation from full dataset, that is, WT and Var samples combined. **E–G,** Network scores as in A–C from $n = 58$ stage I endometrioid-type endometrial tumors; networks generated independently from full dataset. **E,** Tumor scores for metabolic signaling network associated with AMPK and lipid metabolism signaling. **F,** Tumor scores for phospho-AMPKα1 only. **G,** Tumor scores for glucose metabolism-associated network. **H,** Points represent AMPK network score for individual tumors based on rs3820282 genotype and race/ethnicity groups. *, adj.$P < 0.1$, ANOVA with Welch correction. Cells were transfected with siRNA for 72 hours prior to immunoblotting, with ovarian cancer cell lines (**I**) and ILC cell lines (**J**). Representative band from total protein staining shown as loading control.

gynecologic tumor data parallel our observations in ILC and support that WNT4 underpins metabolic remodeling.

We also performed a parallel subset analysis of the largest tumor type in the cohort, stage I endometrioid-type endometrial tumors ($n = 58$ tumors; $n = 190$ differential RPPA targets in WT vs. variant samples). As in the full cohort, variant genotype samples ($n = 29$) showed increased AMPK signaling activation, albeit more modest, but the associated STRING network also included increased lipid metabolism proteins (Fig. 8E and F). WT tumors showed significantly increased glucose metabolism signaling as in the full cohort (Fig. 8G).

With the unique strength of our protein array study in enrichment for tumor samples from non-White patients, we explored how the AMPK network linked to the rs3820282 variant was further linked to ethnic background. We confirmed that an expanded AMPK network ($n = 26$ targets; Supplementary Data S8) was elevated in variant genotype samples in both White (W) and non-White (NW) patient populations; however, AMPK network score was highest specifically in the non-White variant genotype tumors (Fig. 8H). Individual network protein signals were overall higher in the non-White sample set (Supplementary Data S8), for example, pAMPKα2_S345 (variant allele non-White vs. White: mean Z-score difference = 0.63, ANOVA adj.$P = 0.0195$).

We confirmed the link between WNT4 genotype, AMPK activation, and lipid metabolism signaling in cell line models. WNT4 knockdown suppressed phosphorylation of AMPK at T172 in OVSAHO (variant genotype), but not in OVCA429 (WT; Fig. 8I). Phosphorylation of AMPK target ACC was modestly decreased in OVSAHO; AMPK and ACC phosphorylation were both suppressed by WNT4 knockdown in ILC cell lines MM134 and SUM44PE (Fig. 8J). These data support the putative mechanistic links between WNT4 and metabolic signaling identified in patient tumor RPPA, and reinforce that WNT4 signaling is a shared mechanism between ILC and gynecologic tumors.

Discussion

WNT4 plays a unique role in organogenesis, development, and pathology in female reproductive tissues, but mechanisms of *WNT4* dysregulation and downstream signaling are not broadly well understood, due in large part to myriad tissue-specific effects of WNT4 (1). Our observations integrate proteomic, metabolomic, and transcriptomic studies in cell lines, primary human tumor samples, and various public datasets and suggest that convergent mechanisms of WNT4 dysregulation drive cancer metabolism. WNT4 dysregulation occurs via ER in ILC (5) and via SNP rs3820282 in gynecologic cancers (ref. 22; *bioRxiv* 2022.10.25.513653), both resulting in WNT4 dependence and underpinning a critical role for WNT4 in cellular metabolism. We show that WNT4 acts via a novel intracellular mechanism, localizing to the mitochondria instead of canonical secretory/paracrine signaling, ultimately leading to metabolic remodeling with a decrease in glucose metabolism but increase in lipid and/or amino acid metabolism in both ILC and gynecologic cancers.

WNT4 localization to the mitochondria as predicted by BioID links our prior discovery of atypical intracellular localization and function of WNT4 (24), with our findings on WNT4 regulation of mTOR signaling and mitochondrial dynamics (6). In the latter study, we found WNT4 is integral for mTOR signaling via S6 Kinase; WNT4 was necessary for S6 Kinase and S6 phosphorylation, but not mTOR phosphorylation. In the current study, we identified mTOR as a WNT4-associated protein. BioID is limited in not distinguishing proximity versus direct interaction, but WNT4 may regulate mTOR interaction with or access to partners like S6 Kinase. Our observations indicate previously unreported mechanistic links between WNT4, DHRS2, and STAT1. Notably, both DHRS2 and STAT1 are implicated in mitochondrial function and metabolism (36–38, 42, 43); WNT4 association with DHRS2 in particular may regulate fatty acid metabolism and availability for oxidation (43). Future studies will define the discrete localization of WNT4 at/within the mitochondria, trafficking mechanisms, and direct protein interactions. Defining various tissue-specific WNT4 activities as canonical, noncanonical, or atypical/intracellular will be key future directions. In addition, future studies will need to determine how AMPK and ACC signaling, as identified in our protein array studies, are direct targets of WNT4 or are indirect targets or secondary changes, for example, downstream of mTOR signaling and/or direct effects of WNT4 at the mitochondria.

WNT4 has parallel roles in organogenesis and development in the mammary gland and gynecologic tissues, while ILC and gynecologic cancers including ovarian cancer also share intriguing parallels, perhaps most notably their interactions with the microenvironment. Strikingly, ILC metastasize to unique sites relative to other breast cancer, in part mimicking the spread of gynecologic cancer; ILC can spread to the peritoneum, gastrointestinal tract, ovary, and endometrium (44–46). Similarly, data from laboratory models, tumor studies, and clinical imaging studies support that ILC and gynecologic cancers have distinct metabolic phenotypes which preferentially utilize fuels beyond glucose. In ILC, limited FDG avidity in PET-CT imaging strongly suggests ILC tumors preferentially utilize fuels other than glucose, such as amino acids and/or fatty acids. Studies support that ILC cell lines are uniquely dependent on glutamate uptake and metabolism (19, 20). Moreover, upregulation of *SREBP* and *FASN* are critical to antiestrogen resistance in ILC [which also requires WNT4 (5)]; endocrine-resistant ILC cell lines were hypersensitive to SREBP knockdown or inhibition versus parental cells (18). Similarly, ovarian cancer progression relies on fatty acid metabolism, and *FASN* upregulation in ovarian tumors correlates to shorter overall survival (25). In tissue microarray analyses (ILC $n = 108$, IDC $n = 584$), nearly all ILC were positive for hormone-sensitive lipase (HSL/*LIPE*), which hydrolyzes triglycerides into free fatty acids, while this was uncommon in IDC (HSL+: 93% ILC vs. 15% IDC; ref. 17). Fatty acid transporter FABP4 was expressed in 32% of ILC versus <2% of IDC, supporting that ILC require greater fatty acid utilization than IDC. FABP4 expression in ovarian cancer also promotes disease progression and chemoresistance (25, 47). Our analyses of WNT4 signaling support that WNT4 underpins fatty acid metabolism, yet limited data exist to define how this metabolic remodeling is initiated. Notably, recent work shows that the tumor microenvironment and metastatic niche can dramatically reprogram ER-driven cellular metabolism (48). WNT4 signaling may integrate hormonal and/or microenvironmental signals to regulate metabolism in both ILC and gynecologic cancers.

Germline *WNT4* SNPs are linked to 10%–25% increased risk for gynecologic pathologies including endometriosis, leiomyoma, and ovarian cancer (1). Kuchenbaecker and colleagues showed that *WNT4* SNPs (e.g., rs3820282) are associated with an OR for overall ovarian cancer of 1.11 ($P = 8 \times 10^{-7}$), OR = 1.09 for the endometrioid histotype ($P = 0.05$), OR = 1.12 for the serous histotype ($P = 6 \times 10^{-6}$), and OR = 1.24 for the clear cell histotype ($P = 5 \times 10^{-4}$; ref. 49). Critically, rs3820282 VAF varies across ethnic populations: 0%–6% in Black populations; 12%–20% in Caucasian populations; 10%–40% in Latinx populations; 45%–55% in East Asian populations (23). Our data support that the SNP has implications beyond risk, in tumor biology including WNT4 signaling and metabolic remodeling. As such, *WNT4* genotype may drive disparities in ovarian cancer risk, but also create opportunities for precision treatments targeting WNT4 signaling and/or metabolism based on genotype. Future study of WNT4 in ovarian cancer biology (and other gynecologic cancers) are critical to link *WNT4* genotype to cancer risk, patient prognosis, therapy response, patient outcomes, and cancer health disparities. Functional studies of the rs3820282 variant specifically must also dissect the mechanism by which the variant allele activates *WNT4* and associated signaling. It is likely that the variant alters the regulatory context beyond just increasing *WNT4* expression; for example, in knock-in mice with rs3820282 variant genotype versus WT littermates, increased *Wnt4* expression in uterine tissue in was more pronounced in proestrus over estrus (*bioRxiv* 2022.10.25.513653). While ERα likely

plays a role (5, 22), other nuclear receptor-class transcription factors may bind the variant site as well. Key transcription factors may provide critical context to define the impact of *WNT4* genotype in individual patient tumors. Given the increased cancer risks associated with *WNT4* SNPs, developing mechanistic links between *WNT4* genotype, signaling, and cancer progression is also critical.

WNT4 regulates breast and gynecologic cancer metabolism via a previously unappreciated intracellular signaling mechanism at the mitochondria, with WNT4 mediating metabolic remodeling favoring lipid metabolism. Understanding how WNT4 signaling is dysregulated, by estrogen and genetic polymorphism in ILC vs. gynecologic cancers, offers new opportunities for defining tumor biology, precision therapeutics, and personalized cancer risk assessment.

Authors' Disclosures

S. Oesterreich has received funding from NCI, Komen, and BCRF for research on ILC but these are not of relevance to the here described work. Z. Madak-Erdogan reports other from Endocrine Society and Elsevier, grants from Karyopharm Therapeutics outside the submitted work. R.B. Riggins reports grants from CDMRP Breast Cancer Research Program during the conduct of the study. B.R. Corr reports other from GSK, Gilead, Immunogen, Zentalis, Merck, Corcept, Imvax, Clovis, and Immunogen outside the submitted work. B.G. Bitler reports grants from NCI/NIH, ACS, DOD, and OCRA during the conduct of the study; other from Onconic Therapeutics outside the submitted work. M.J. Sikora reports grants from NCI, Cancer League of Colorado, Golfers Against Cancer, University of Colorado Cancer Center, and Ovarian Cancer Research Alliance during the conduct of the study. No disclosures were reported by the other authors.

Authors' Contributions

J.L. Sottnik: Formal analysis, validation, investigation, methodology, writing-review and editing. **M.T. Shackleford:** Formal analysis, validation, investigation, methodology, writing-review and editing. **S.K. Robinson:** Investigation, methodology, writing-review and editing. **F.R. Villagomez:** Investigation, methodology, writing-review and editing. **S. Bahnassy:** Formal analysis, investigation, writing-review and editing. **S. Oesterreich:** Resources, formal analysis, writing-review and editing. **J. Hu:** Formal analysis, writing-review and editing. **Z. Madak-Erdogan:** Formal analysis, writing-review and editing. **R.B. Riggins:** Formal analysis, writing-review and editing. **B.R. Corr:** Formal analysis, writing-review and editing. **L.S. Cook:** Formal analysis, methodology, writing-review and editing. **L.S. Treviño:** Formal analysis, methodology, writing-review and editing. **B.G. Bitler:** Conceptualization, resources, formal analysis, supervision, funding acquisition, investigation, methodology, writing-review and editing. **M.J. Sikora:** Conceptualization, resources, data curation, formal analysis, supervision, funding acquisition, validation, investigation, visualization, methodology, writing-original draft, writing-review and editing.

Acknowledgments

The authors wish to thank Dr. Julie Haines and the University of Colorado School of Medicine Metabolomics Core, and Dr. Chris Ebmeier and the Central Analytical Mass Spectrometry Facility at the University of Colorado Boulder, for their contributions to this project. We thank the University of Colorado Anschutz Medical Campus Cancer Center Pathology Shared Resource Biorepository Core Facility (RRID:SCR_021989) for support with tumor tissue banking. We thank Dr. Courtney Jones and the Craig Jordan Laboratory for technical assistance with Seahorse metabolic flux analyses. We acknowledge philanthropic contributions from Kay L. Dunton Endowed Memorial Professorship in Ovarian Cancer Research, the McClintock-Addlesperger Family, Karen M. Jennison, Don and Arlene Mohler Johnson Family, Michael Intagliata, Duane and Denise Suess, Mary Normandin, and Donald Engelstad.

This work was supported by R00 CA193734 (M.J. Sikora) from the NIH, by a grant from the Cancer League of Colorado, Inc (#173664-MS, M.J. Sikora), by a grant from the Denver Chapter of Golfers Against Cancer (2021 Pilot Award, M.J. Sikora) and by support from the Tumor-Host Interactions Program at the University of Colorado Cancer Center (AWD63502622 to M.J. Sikora; THI.2023.008-COE to M.J. Sikora and B.G. Bitler). This work was supported by grants from the Ovarian Cancer Research Alliance (M.J. Sikora and B.G. Bitler; 2022 Collaborative Award), the Department of Defense (B.G. Bitler: OC170228, OC200302, OC200225), the NIH/NCI (B.G. Bitler, R37 CA261987; M.J. Sikora and B.G. Bitler, R01 CA285446), and the American Cancer Society (B.G. Bitler, 134106-RSG-19-129-01-DDC), as well as the University of Colorado Chancellor's Discovery Fund (B.G. Bitler), OB-GYN Academic Enrichment Fund (B.G. Bitler), and Gynecologic Oncology Academic Enrichment Fund (B.G. Bitler). This work was supported by the Office of the Assistant Secretary of Defense for Health Affairs through the Breast Cancer Research Program under Award No. W81XWH-17-1-0615 (R.B. Riggins). This study utilized University of Colorado Cancer Center shared resources, which are supported in part by the NCI through Cancer Center Support Grant P30CA046934. This study utilized the Central Analytical Mass Spectrometry Facility at the University of Colorado Boulder, supported in part by the National Institutes of Health support grant S10OD025267. Opinions, interpretations, conclusions, and recommendations are those of the authors and are not necessarily endorsed by the Department of Defense or the NIH.

Note

Supplementary data for this article are available at Cancer Research Communications Online (https://aacrjournals.org/cancerrescommun/).

Received June 21, 2023; revised October 31, 2023; accepted December 13, 2023; published first January 17, 2024.

References

1. Pitzer LM, Moroney MR, Nokoff NJ, Sikora MJ. WNT4 balances development vs disease in gynecologic tissues and women's health. Endocrinology 2021;162: bqab093.
2. Alexander CM, Goel S, Fakhraldeen SA, Kim S. Wnt signaling in mammary glands: plastic cell fates and combinatorial signaling. Cold Spring Harb Perspect Biol 2012;4: a008037.

3. Brisken C, Hess K, Jeitziner R. Progesterone and overlooked endocrine pathways in breast cancer pathogenesis. Endocrinology 2015;156: 3442-50.
4. Sikora MJ, Cooper KL, Bahreini A, Luthra S, Wang G, Chandran UR, et al. Invasive lobular carcinoma cell lines are characterized by unique estrogen-mediated gene expression patterns and altered tamoxifen response. Cancer Res 2014;74: 1463-74.
5. Sikora MJ, Jacobsen BM, Levine K, Chen J, Davidson NE, Lee AV, et al. WNT4 mediates estrogen receptor signaling and endocrine resistance in invasive lobular carcinoma cell lines. Breast Cancer Res 2016;18: 92.
6. Shackleford MT, Rao DM, Bordeaux EK, Hicks HM, Towers CG, Sottnik JL, et al. Estrogen regulation of mTOR signaling and mitochondrial function in invasive lobular carcinoma cell lines requires WNT4. Cancers (Basel) 2020;12: 2931.
7. Ciriello G, Gatza ML, Beck AH, Wilkerson MD, Rhie SK, Pastore A, et al. Comprehensive molecular portraits of invasive lobular breast cancer. Cell 2015;163: 506-19.
8. Fujii T, Yajima R, Kurozumi S, Higuchi T, Obayashi S, Tokiniwa H, et al. Clinical significance of 18F-FDG-PET in invasive lobular carcinoma. Anticancer Res 2016;36: 5481-5.
9. Ulaner GA, Jhaveri K, Chandarlapaty S, Hatzoglou V, Riedl CC, Lewis JS, et al. Head-to-head evaluation of 18F-FES and 18F-FDG PET/CT in metastatic invasive lobular breast cancer. J Nucl Med 2021;62: 326-31.
10. Hogan MP, Goldman DA, Dashevsky B, Riedl CC, Gönen M, Osborne JR, et al. Comparison of 18F-FDG PET/CT for systemic staging of newly diagnosed invasive lobular carcinoma versus invasive ductal carcinoma. J Nucl Med 2015;56: 1674-80.
11. Ulaner GA, Goldman DA, Gönen M, Pham H, Castillo R, Lyashchenko SK, et al. Initial results of a prospective clinical trial of 18F-fluciclovine PET/CT in newly diagnosed invasive ductal and invasive lobular breast cancers. J Nucl Med 2016;57: 1350-6.
12. Ueda S, Tsuda H, Asakawa H, Shigekawa T, Fukatsu K, Kondo N, et al. Clinicopathological and prognostic relevance of uptake level using 18F-fluorodeoxyglucose positron emission tomography/computed tomography fusion imaging (18F-FDG PET/CT) in primary breast cancer. Jpn J Clin Oncol 2008;38: 250-8.
13. Venema C, de Vries E, Glaudemans A, Poppema B, Hospers G, Schröder C. 18F-FES PET has added value in staging and therapy decision making in patients with disseminated lobular breast cancer. Clin Nucl Med 2017;42: 1.
14. Ravina M, Saboury B, Chauhan MS, Jacob MJ, Pandit AG, Sanchety N, et al. Utility of 18 F-FDG PET/CT in pre-surgical risk stratification of patients with breast cancer. Hell J Nucl Med 2019;22: 165-71.
15. Du T, Zhu L, Levine KM, Tasdemir N, Lee AV, Vignali DAA, et al. Invasive lobular and ductal breast carcinoma differ in immune response, protein translation efficiency and metabolism. Sci Rep 2018;8: 7205.
16. Kim YH, Jung WH, Koo JS. Expression of metabolism-related proteins in invasive lobular carcinoma: comparison to invasive ductal carcinoma. Tumour Biol 2014;35: 10381-93.
17. Cha YJ, Kim HM, Koo JS. Expression of Lipid metabolism-related proteins differs between invasive lobular carcinoma and invasive ductal carcinoma. Int J Mol Sci 2017;18: 232.
18. Du T, Sikora MJ, Levine KM, Tasdemir N, Riggins RB, Wendell SG, et al. Key regulators of lipid metabolism drive endocrine resistance in invasive lobular breast cancer. Breast Cancer Res 2018;20: 106.
19. Stires H, Heckler MM, Fu X, Li Z, Grasso CS, Quist MJ, et al. Integrated molecular analysis of Tamoxifen-resistant invasive lobular breast cancer cells identifies MAPK and GRM/mGluR signaling as therapeutic vulnerabilities. Mol Cell Endocrinol 2018;471: 105-17.
20. Olukoya AO, Stires H, Bahnassy S, Persaud S, Guerra Y, Ranjit S, et al. Riluzole suppresses growth and enhances response to endocrine therapy in ER+ breast cancer. J Endocr Soc 2023;7: bvad117.
21. Luong HTT, Painter JN, Shakhbazov K, Chapman B, Henders AK, Powell JE, et al. Fine mapping of variants associated with endometriosis in the WNT4 region on chromosome 1p36. Int J Mol Epidemiol Genet 2013;4: 193-206.
22. Zhang G, Feenstra B, Bacelis J, Liu X, Muglia LM, Juodakis J, et al. Genetic associations with gestational duration and spontaneous preterm birth. N Engl J Med 2017;377: 1156-67.
23. Fairley S, Lowy-Gallego E, Perry E, Flicek P. The international genome sample resource (IGSR) collection of open human genomic variation resources. Nucleic Acids Res 2020;48: D941-7.
24. Rao DM, Shackleford MT, Bordeaux EK, Sottnik JL, Ferguson RL, Yamamoto TM, et al. Wnt family member 4 (WNT4) and WNT3A activate cell-autonomous Wnt signaling independent of porcupine O-acyltransferase or Wnt secretion. J Biol Chem 2019;294: 19950-66.
25. Wheeler LJ, Watson ZL, Qamar L, Yamamoto TM, Sawyer BT, Sullivan KD, et al. Multi-omic approaches identify metabolic and autophagy regulators important in ovarian cancer dissemination. iScience 2019;19: 474-91.
26. Yamamoto TM, McMellen A, Watson ZL, Aguilera J, Ferguson R, Nurmemmedov E, et al. Activation of Wnt signaling promotes olaparib resistant ovarian cancer. Mol Carcinog 2019;58: 1770-82.
27. Sottnik JL, Bordeaux EK, Mehrotra S, Ferrara SE, Goodspeed AE, Costello JC, et al. Mediator of DNA damage checkpoint 1 (MDC1) is a novel estrogen receptor coregulator in invasive lobular carcinoma of the breast. Mol Cancer Res 2021;19: 1270-82.
28. Liu X, Salokas K, Tamene F, Jiu Y, Weldatsadik RG, Öhman T, et al. An AP-MS- and BioID-compatible MAC-tag enables comprehensive mapping of protein interactions and subcellular localizations. Nat Commun 2018;9: 1188.
29. Shah AD, Goode RJA, Huang C, Powell DR, Schittenhelm RB. LFQ-analyst: an easy-to-use interactive web platform to analyze and visualize label-free proteomics data preprocessed with MaxQuant. J Proteome Res 2020;19: 204-11.
30. Mellacheruvu D, Wright Z, Couzens AL, Lambert JP, St-Denis NA, Li T, et al. The CRAPome: a contaminant repository for affinity purification-mass spectrometry data. Nat Methods 2013;10: 730-6.
31. Xie Z, Bailey A, Kuleshov MV, Clarke DJB, Evangelista JE, Jenkins SL, et al. Gene set knowledge discovery with enrichr. Curr Protoc 2021;1: e90.
32. Sherman BT, Hao M, Qiu J, Jiao X, Baseler MW, Lane HC, et al. DAVID: a web server for functional enrichment analysis and functional annotation of gene lists (2021 update). Nucleic Acids Res 2022;50: W216-21.
33. Orre LM, Vesterlund M, Pan Y, Arslan T, Zhu Y, Fernandez Woodbridge A, et al. SubCellBarCode: proteome-wide mapping of protein localization and relocalization. Mol Cell 2019;73: 166-82.e7.
34. Pang Z, Zhou G, Ewald J, Chang L, Hacariz O, Basu N, et al. Using MetaboAnalyst 5.0 for LC-HRMS spectra processing, multi-omics integration and covariate adjustment of global metabolomics data. Nat Protoc 2022;17: 1735-61.
35. Jones CL, Stevens BM, D'Alessandro A, Reisz JA, Culp-Hill R, Nemkov T, et al. Inhibition of amino acid metabolism selectively targets human leukemia stem cells. Cancer Cell 2018;34: 724-40.e4.
36. Meier JA, Larner AC. Toward a new STATe: the role of STATs in mitochondrial function. Semin Immunol 2014;26: 20-8.
37. Sisler JD, Morgan M, Raje V, Grande RC, Derecka M, Meier J, et al. The signal transducer and activator of transcription 1 (STAT1) inhibits mitochondrial biogenesis in liver and fatty acid oxidation in adipocytes. PLoS One 2015;10: e0144444.
38. Bourke LT, Knight RA, Latchman DS, Stephanou A, McCormick J. Signal transducer and activator of transcription-1 localizes to the mitochondria and modulates mitophagy. JAKSTAT 2013;2: e25666.
39. Tsherniak A, Vazquez F, Montgomery PG, Weir BA, Kryukov G, Cowley GS, et al. Defining a cancer dependency map. Cell 2017;170: 564-76.e16.
40. Michaut M, Chin SF, Majewski I, Severson TM, Bismeijer T, de Koning L, et al. Integration of genomic, transcriptomic and proteomic data identifies two biologically distinct subtypes of invasive lobular breast cancer. Sci Rep 2016;6: 18517.
41. Szklarczyk D, Gable AL, Lyon D, Junge A, Wyder S, Huerta-Cepas J, et al. STRING v11: protein-protein association networks with increased coverage, supporting functional discovery in genome-wide experimental datasets. Nucleic Acids Res 2019;47: D607-13.
42. Monge M, Colas E, Doll A, Gil-Moreno A, Castellvi J, Diaz B, et al. Proteomic approach to ETV5 during endometrial carcinoma invasion reveals a link to oxidative stress. Carcinogenesis 2009;30: 1288-97.
43. Luo X, Li N, Zhao X, Liao C, Ye R, Cheng C, et al. DHRS2 mediates cell growth inhibition induced by Trichothecin in nasopharyngeal carcinoma. J Exp Clin Cancer Res 2019;38: 300.

44. Mouabbi JA, Hassan A, Lim B, Hortobagyi GN, Tripathy D, Layman RM. Invasive lobular carcinoma: an understudied emergent subtype of breast cancer. Breast Cancer Res Treat 2022;193: 253-64.
45. Arpino G, Bardou VJ, Clark GM, Elledge RM. Infiltrating lobular carcinoma of the breast: tumor characteristics and clinical outcome. Breast Cancer Res 2004;6: R149-56.
46. Mathew A, Rajagopal PS, Villgran V, Sandhu GS, Jankowitz RC, Jacob M, et al. Distinct pattern of metastases in patients with invasive lobular carcinoma of the breast. Geburtshilfe Frauenheilkd 2017;77: 660-6.
47. Gansler TS, Hardman W, Hunt DA, Schaffel S, Hennigar RA. Increased expression of fatty acid synthase (OA-519) in ovarian neoplasms predicts shorter survival. Hum Pathol 1997;28: 686-92.
48. Zuo Q, Mogol AN, Liu YJ, Santaliz Casiano A, Chien C, Drnevich J, et al. Targeting metabolic adaptations in the breast cancer-liver metastatic niche using dietary approaches to improve endocrine therapy efficacy. Mol Cancer Res 2022; 1-15.
49. Kuchenbaecker KB, Ramus SJ, Tyrer J, Lee A, Shen HC, Beesley J, et al. Identification of six new susceptibility loci for invasive epithelial ovarian cancer. Nat Genet 2015;47: 164-71.